*Int. J. Heat Mass Transfer.* Vol. 28, No. 2, pp. 441–449, 1985
Printed in Great Britain

0017-9310/85 $3.00 + 0.00
Pergamon Press Ltd.

# Effects of anisotropic scattering on melting and solidification of a semi-infinite, semi-transparent medium

F. O. ORUMA
Department of Mechanical and Aerospace Engineering, North Carolina State University, Raleigh, N.C 27650, U.S.A.

and

M. N. ÖZIŞIK*
Institut für Verfahrens-und Kaltechnik, ETH-Zentrum, CH-8092 Zürich

and

M. A. BOLES
Department of Mechanical and Aerospace Engineering, North Carolina State University, Raleigh, N.C 27650, U.S.A.

(*Received* 27 *June* 1983; *in final form* 20 *February* 1984)

**Abstract**—The effects of anisotropic scattering of radiation on the melting (solidification) of a semi-infinite, semi-transparent medium at melting temperature is investigated. The model allows for the penetration of radiation deep into the isothermal region causing local melting, hence generating a two-phase zone between the purely liquid and purely solid regions. The results show that anisotropic scattering has significant effects on the rate of propagation of the melt (solidification) front. Backward scattering retards the melting, while forward scattering enhances it. The more forward the scattering, the faster the rate of melting (solidification) of the medium.

## INTRODUCTION

THE EFFECT of radiation on the melting and solidification of semi-transparent materials is important in many practical heat-transfer problems. Applications include the design of certain latent heat-of-fusion thermal-storage systems [1], the prediction of ice melting rates [2], laser annealing of solar cell wafers [3] and semiconductor crystal growth. The exact and approximate methods of solving one-dimensional melting or solidification problem for an opaque, semi-infinite region is well documented in the literature [4, 5]. In the case of semi-transparent materials, most investigations have considered purely black-body radiation [6, 7, 8] or isotropic scattering [9, 10]. Recently, Diaz *et al.* [11, 12] utilized a non-gray model to investigate the one-dimensional melting of *n*-octadecane due to an external radiation source. Highly peaked forward scattering is assumed for the radiation problem and the emission of radiation from the medium was neglected.

It appears that the effects of anisotropic scattering on melting and solidification have not been demonstrated. Moreover, the existing studies use the standard formulation which consists of purely liquid and purely solid regions. The model utilized here allows for the existence of a two-phase zone between the purely liquid and purely solid regions, resulting from the penetration of radiation deep into the isothermal region which causes local melting (solidification) ahead of the melt (solid) front [8]. The objective of this work is to study the effects of general anisotropic scattering on the melting and solidification of a semi-infinite semi-transparent medium by using various scattering laws. The scattering laws considered here include one case of backward scattering, three different cases of forward scattering [13], and the isotropic scattering that formed the basis for the comparison of effects of anisotropy.

## PROBLEM FORMULATION

Consider the melting of a semi-infinite, semi-transparent solid initially at the melting temperature $T_m$, confined to the domain $x \geqslant 0$. The medium is homogeneous and isotropic. It absorbs, emits and anisotropically scatters the radiation and has constant thermo-physical properties everywhere. At $t = 0$, the temperature at the boundary surface $x = 0$ is suddenly raised to $T_0$, which is higher than the melting temperature $T_m$ of the solid, and afterwards maintained at that temperature. Figure 1 illustrates the geometry and coordinates. The mathematical formulation of this phase-change problem is given in the dimensionless form as:

* Permanent address: Department of Mechanical and Aerospace Engineering, North Carolina State University, Raleigh, N.C 27650, U.S.A.

## NOMENCLATURE

| | |
|---|---|
| $c_L$ | specific heat |
| $D$ | diameter of scattering particle |
| $H(\xi)$ | $h(t)/X_0$, dimensionless location of interface |
| $h(t)$ | location of interface |
| $I(x,\mu)$ | radiation intensity |
| $k$ | thermal conductivity |
| $L$ | latent heat of fusion |
| $n$ | refractive index |
| $N_L$ | $k_L\beta_L/4n^2\bar{\sigma}T_m^3$, conduction-to-radiation parameter |
| $Q^r$ | $q^r/4n^2\bar{\sigma}T_m^4$, dimensionless net radiation flux |
| $q^r$ | net radiation heat flux |
| $S_L$ | $c_LT_m/L$, Stefan number |
| $T(x,t)$ | temperature |
| $T_m, T_0$ | melt and wall temperatures, respectively |
| $t$ | time |
| $X_D$ | $\pi D/\lambda$, scattering cross-section |
| $X_0$ | a reference length |
| $x$ | axial distance. |

Greek letters

| | |
|---|---|
| $\alpha_L$ | $k_L/\rho_Lc_L$, thermal diffusivity |
| $\beta$ | extinction coefficient |
| $\gamma$ | void fraction |
| $\varepsilon$ | emissivity |
| $\eta$ | $x/X_0$, dimensionless axial distance |
| $\theta(\eta,\xi)$ | $T(x,t)/T_m$, dimensionless temperature |
| $\theta_0$ | $T_0/T_m$, dimensionless wall temperature |
| $\kappa$ | absorption coefficient |
| $\lambda$ | wavelength of incident radiation |
| $v_j, v$ | discrete and continuum eigenvalues |
| $\xi$ | $\alpha_Lt/X_0^2$, dimensionless time |
| $\rho$ | density |
| $\bar{\sigma}$ | Stefan–Boltzmann constant |
| $\tau$ | optical thickness |
| $\omega$ | single scattering albedo. |

Subscripts

| | |
|---|---|
| $L$ | liquid phase |
| $S$ | solid phase |
| $m$ | melting point. |

*Liquid phase*

$$\frac{\partial^2\theta_L(\eta,\xi)}{\partial\eta^2}-\frac{1}{N_L}\frac{\partial Q^r(\eta,\xi)}{\partial\eta}=\frac{\partial\theta_L(\eta,\xi)}{\partial\xi} \quad \text{in } 0<\eta<H(\xi),\ \xi>0 \tag{1a}$$

$$\theta_L(0,\xi)=\theta_0 \quad \text{for} \quad \xi>0 \tag{1b}$$

$$\theta_L(H,\xi)=1 \quad \text{for} \quad \xi>0 \tag{1c}$$

*Liquid–solid interface*

$$\frac{S_L}{(1-\gamma|_{H^+})}\left[-\frac{\partial\theta_L(\eta,\xi)}{\partial\eta}+\frac{1}{N_L}(Q^r|_{H^-}-Q^r|_{H^+})\right]=\frac{dH(\xi)}{d\xi} \tag{2a}$$

$$H(\xi)=0 \quad \text{for} \quad \xi=0 \tag{2b}$$

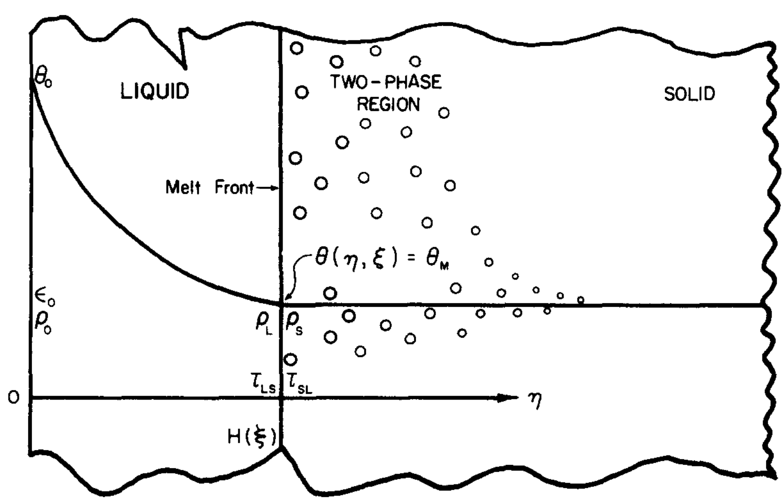


FIG. 1. The geometry and coordinates.

where $\gamma$ is the voidage (i.e. the fraction of liquid in solid per unit volume). The notation $H^+$ implies a position immediately on the right-hand side of the liquid–solid interface $H(\xi)$ illustrated in Fig. 1. Clearly, for a transparent interface $Q^r|_{H^-} - Q^r|_{H^+} = 0.0$ or the radiation has no affect on the interface condition.

*Two-phase zone*

$$\frac{\mathrm{d}\gamma(\eta,\xi)}{\mathrm{d}\xi} = -\frac{S_L}{N_L}\frac{\partial Q^r(\eta,\xi)}{\partial \eta}, \quad \text{in} \quad \eta > H(\xi) \quad (3a)$$

$$\gamma(\eta,\xi) = 0 \quad \text{for} \quad \xi = 0 \quad (3b)$$

$$\gamma(\eta,\xi) \to 0 \quad \text{as} \quad \eta \to \infty \quad (3c)$$

where, various dimensionless quantities are defined as

$$\left.\begin{aligned} \theta(\eta,\xi) &= \frac{T(x,t)}{T_m}, \quad \theta_0 = \frac{T_0}{T_m}, \quad \xi = \frac{\alpha_L t}{X_0^2} \\ \eta &= \frac{x}{X_0}, \quad \alpha_L = \frac{k_L}{\rho_L c_L}, \quad N_L = \frac{k_L \beta_L}{4n^2\bar{\sigma}T_m^3} \\ H(\xi) &= \frac{h(t)}{X_0}, \quad Q^r = \frac{q^r}{4n^2\bar{\sigma}T_m^4}, \quad S_L = \frac{c_L T_m}{L} \end{aligned}\right\} \quad (4)$$

and the dimensionless radiation heat flux $Q^r(\eta,\xi)$ is related to the dimensionless radiation intensity $\psi(\eta,\mu)$ by

$$Q^r(\eta,\xi) = \frac{1}{2}\int_{-1}^{1} \psi(\eta,\mu)\mu \,\mathrm{d}\mu \quad (5a)$$

where

$$\psi(\eta,\mu) = I(\eta,\mu)\Big/\left(\frac{n^2\bar{\sigma}T_m^4}{\pi}\right). \quad (5b)$$

For the radiation part of the problem, we assume one dimensional, plane-parallel, absorbing, emitting and anisotropically scattering medium. Then the dimensionless radiation intensity $\psi(\tau,\mu)$ in the optical variable, $\tau$, satisfies the following radiation problem:

*Equation for the liquid region*

$$\mu\frac{\partial \psi_L(\tau,\mu)}{\partial \tau} + \psi_L(\tau,\mu) = S_L(\tau),$$

$$\text{in } 0 < \tau < H(\xi), \; -1 \leqslant \mu \leqslant 1 \quad (6a)$$

where

$$S_L(\tau) = (1-\omega)\theta_L^4(\eta,\xi) + \frac{\omega}{2}\int_{-1}^{1} p(\mu_0)\psi_L(\tau,\mu')\,\mathrm{d}\mu' \quad (6b)$$

*Equation for the solid region*

$$\mu\frac{\partial \psi_S(\tau,\mu)}{\partial \tau} + \psi_S(\tau,\mu) = S_S(\tau)$$

$$\text{in } H(\xi) < \tau < \infty, \; -1 \leqslant \mu \leqslant 1 \quad (7a)$$

where

$$S_S(\tau) = (1-\omega) + \frac{\omega}{2}\int_{-1}^{1} p(\mu_0)\psi_S(\tau,\mu')\,\mathrm{d}\mu' \quad (7b)$$

and the phase function $p(\mu_0)$ is expressed as

$$p(\mu_0) = 1 + \sum_{j=1}^{M} f_j P_j(\mu_0) \quad (7c)$$

*The boundary conditions*

$$\psi_L(0,\mu) = \varepsilon_0\theta_0^4 + 2\rho_0\int_0^1 \mu'\psi_L(0,-\mu')\,\mathrm{d}\mu', \quad \mu > 0 \quad (8a)$$

$$\psi_L(H,-\mu) = \tau_{SL}\psi_S(H,-\mu) + 2\rho_L\int_0^1 \mu'\psi_L(H,\mu')\,\mathrm{d}\mu', \quad \mu > 0 \quad (8b)$$

$$\psi_S(H,\mu) = \tau_{LS}\psi_L(H,\mu) + 2\rho_S\int_0^1 \mu'\psi_S(H,-\mu')\,\mathrm{d}\mu', \quad \mu > 0 \quad (8c)$$

$$\psi_S(\tau,\mu) = 1 \quad \text{as} \quad \tau \to \infty \quad (8d)$$

where $\varepsilon_0$ and $\rho_0$ are the emissivity and reflectivity of the boundary surface at $\tau = 0$, respectively; $\rho_L$ and $\rho_S$ are the reflectivity of the interface on the liquid and solid side, respectively; $\tau_{SL}$ and $\tau_{LS}$ are the transmissivity of the interface from the solid-to-liquid side and from the liquid-to-solid side, respectively.

The above equation of radiative transfer includes anisotropic scattering of order $M$; $\mu$ is the direction cosine of the propagating radiation (as measured from the positive $\tau$ axis); and the constants $f_j, j = 0, 1, 2, 3, \ldots, M$ with $f_0 = 1$, are the coefficients in a Legendre expansion of the phase function [14]. The optical variable is related to the physical coordinate $x$ by

$$\tau = \beta x \quad (9a)$$

where $\beta$ is the extinction coefficient. In order to establish a relationship between $\tau$ and the dimensionless coordinate

$$\eta = \frac{x}{X_0} \quad (9b)$$

we choose the reference length as

$$X_0 = \frac{1}{\beta}. \quad (9c)$$

Then $\tau$ and $\eta$ are related by

$$\tau = \eta \quad (9d)$$

or, the optical coordinate $\tau$ and the dimensionless coordinate $\eta$ become identical.

## THE FORMAL SOLUTION

The conduction part of the problem, consisting of equations (1)–(3), is solved by the integral method and the radiation part involving equations (6)–(8) is solved by the application of the $F_N$ method [15, 16].

The integration of equations (1) from $\eta = 0$ to $\eta = H(\xi)$ and using equations (2), yield the energy integral equation as

$$\left[1-\frac{(1-\gamma|_{H^+})}{S_L}\right]\frac{\mathrm{d}H}{\mathrm{d}\xi}=\frac{\mathrm{d}F_L}{\mathrm{d}\xi}+\left.\frac{\partial\theta_L}{\partial\eta}\right|_{\eta=0}-\left.\frac{Q^r}{N_L}\right|_{\eta=0} \tag{10a}$$

where

$$F_L(\eta,\xi)=\int_0^{H(\xi)}\theta_L(\eta,\xi)\,\mathrm{d}\eta. \tag{10b}$$

The liquid-phase temperature profile is now represented with a second-degree polynomial in the form

$$\theta_L(\eta,\xi)=Y_0+Y_1(\eta-H)+Y_2(\eta-H)^2 \tag{11a}$$

where the coefficients in equation (11a) are determined as

$$Y_0=1,\quad Y_1=\frac{\delta-\sqrt{(\delta^2+4\Delta)}}{2}$$

$$\text{and}\quad Y_2=\frac{\theta_0+Y_1H-1}{H^2} \tag{11b}$$

where

$$\delta=\frac{1}{N_L}Q^r|_{\eta=H}+\frac{2(1-\gamma|_{H^+})}{S_LH} \tag{11c}$$

and

$$\Delta=\frac{(1-\gamma|_{H^+})}{S_L}\left[\frac{2(\theta_0-1)}{H^2}-\frac{1}{N_L}\left.\frac{\partial Q^r}{\partial\eta}\right|_H\right]. \tag{11d}$$

This temperature profile is introduced into equation (10) to yield

$$\xi=\int_0^{H(\xi)}\frac{\left[\dfrac{\theta_0-1}{3}-\dfrac{Y_1}{3}H'-\dfrac{H'^2}{6}\dfrac{\mathrm{d}Y_1}{\mathrm{d}H'}+\dfrac{(1-\gamma|_{H^+})}{S_L}\right]}{\left[Y_1H'+2(\theta_0-1)+\dfrac{H'}{N_L}Q^r|_{\eta=0}\right]}\times H'\,\mathrm{d}H'. \tag{12}$$

Given the radiative heat flux $Q^r$, this expression can be used to evaluate the location of the solid–liquid interface. To determine the radiation heat flux, $Q^r$, the radiation part of the problem comprising equations (6)–(8) is solved formally for the dimensionless radiation intensity $\psi(\eta,\mu)$ for an assumed temperature profile and the definition given by equation (5) is utilized. The iteration is carried out until sufficient convergence is achieved. The mathematical details of the solution of the radiation problem is quite lengthy; it is discussed in the Appendix.

## RESULTS AND DISCUSSIONS

The directional distribution of scattered radiation is described by the phase function $p(\mu_0)$, given by equation (7c). The phase functions considered in the present study are listed in Table 1 and shown in Figs 2–5. Figure 2 illustrates a scattering law in which particles scatter more in the backward direction. The laws in Figs 3, 4 and 5 illustrate forward scattering with different magnitudes of scatter in the forward direction. The following results demonstrate the effects of these various scattering laws on the rate of melting.

Table 1. The coefficient $f_j$ in the phase function of the scattering laws [13]

$$p(\mu_0)=1+\sum_{j=1}^{M}f_jP_j(\mu_0)$$

| CASE | A | | B | | C | | | | D | | | | | |
|---|---|---|---|---|---|---|---|---|---|---|---|---|---|---|
| n | ∞ | | 1.6 | | 1.15 | | | | 0.9 | | | | | |
| $X_D$ | 1.0 | | 4.0 | | 15 | | | | 25 | | | | | |
| | j | $f_j$ | j | $f_j$ | j | $f_j$ | j | $f_j$ | j | $f_j$ | j | $f_j$ | j | $f_j$ |
| | 1 | -0.56524 | 1 | 1.93460 | 1 | 2.65809 | 21 | 6.63615 | 1 | 2.92954 | 21 | 12.06216 | 42 | 2.29670 |
| | 2 | 0.29783 | 2 | 2.70129 | 2 | 4.32792 | 22 | 5.74359 | 2 | 4.69271 | 22 | 11.96434 | 43 | 1.77777 |
| | 3 | 0.08571 | 3 | 2.51662 | 3 | 5.65671 | 23 | 4.93859 | 3 | 6.23311 | 23 | 11.83534 | 44 | 1.32202 |
| | 4 | 0.01003 | 4 | 2.63819 | 4 | 6.86793 | 24 | 3.90658 | 4 | 7.53797 | 24 | 11.68176 | 45 | 0.93651 |
| | 5 | 0.00063 | 5 | 2.29733 | 5 | 7.69313 | 25 | 3.03764 | 5 | 8.61451 | 25 | 11.49385 | 46 | 0.62721 |
| | 6 | 0.00000 | 6 | 1.85084 | 6 | 8.47467 | 26 | 2.33309 | 6 | 9.48703 | 26 | 11.26438 | 47 | 0.39461 |
| | | | 7 | 1.25977 | 7 | 8.95965 | 27 | 1.12968 | 7 | 10.18250 | 27 | 10.99902 | 48 | 0.23240 |
| | | | 8 | 0.76693 | 8 | 9.39569 | 28 | 0.70334 | 8 | 10.72784 | 28 | 10.69314 | 49 | 0.12762 |
| | | | 9 | 0.11094 | 9 | 9.65789 | 29 | 0.42134 | 9 | 11.15109 | 29 | 10.33378 | 50 | 0.06524 |
| | | | 10 | 0.02125 | 10 | 9.84110 | 30 | 0.20664 | 10 | 11.47291 | 30 | 9.92466 | 51 | 0.03112 |
| | | | 11 | 0.00320 | 11 | 9.94902 | 31 | 0.08371 | 11 | 11.71835 | 31 | 9.47260 | 52 | 0.01363 |
| | | | 12 | 0.00039 | 12 | 9.92907 | 32 | 0.02942 | 12 | 11.89769 | 32 | 8.96608 | 53 | 0.00564 |
| | | | 13 | 0.00003 | 13 | 9.91779 | 33 | 0.00918 | 13 | 12.03007 | 33 | 8.39732 | 54 | 0.00212 |
| | | | 14 | 0.00000 | 14 | 9.71919 | 34 | 0.00259 | 14 | 12.12181 | 34 | 7.78169 | 55 | 0.00074 |
| | | | | | 15 | 9.58930 | 35 | 0.00065 | 15 | 12.18075 | 35 | 7.13157 | 56 | 0.00022 |
| | | | | | 16 | 9.21888 | 36 | 0.00140 | 16 | 12.21686 | 36 | 6.44003 | 57 | 0.00000 |
| | | | | | 17 | 8.96092 | 37 | 0.00002 | 17 | 12.22693 | 37 | 5.70470 | | |
| | | | | | 18 | 8.39294 | 38 | 0.00000 | 18 | 12.21725 | 38 | 4.94810 | | |
| | | | | | 19 | 8.00209 | | | 19 | 12.18918 | 39 | 4.20739 | | |
| | | | | | 20 | 7.23222 | | | 20 | 12.13448 | 40 | 3.51220 | | |
| | | | | | | | | | | | 41 | 2.87477 | | |

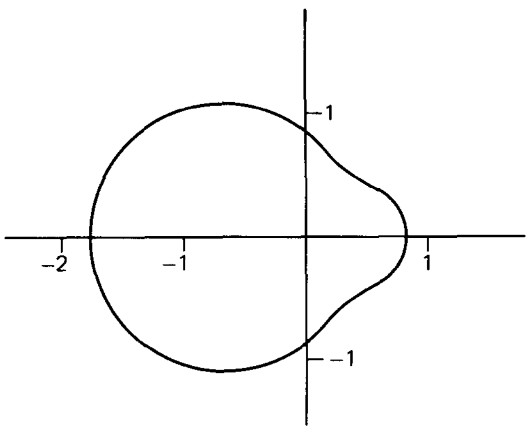


FIG. 2. The phase diagram for backward scattering with $n = \infty$, $X_D = 1.0$ (Table 1, case A).

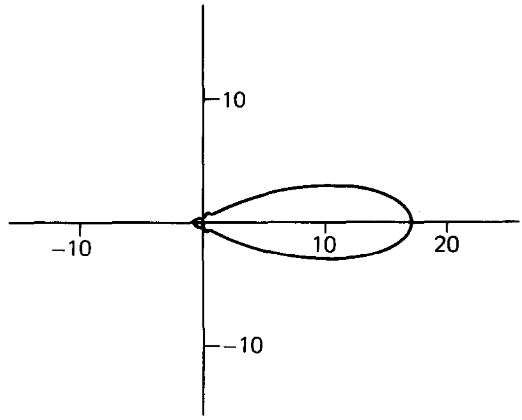


FIG. 3. The phase diagram for forward scattering with $n = 1.6$, $X_D = 4.0$ (Table 1, case B).

To provide a basis for comparing the effects of anisotropic scattering, we first examine the problem of pure radiative heat transfer in a plane parallel slab with transparent boundaries, subjected to an isotropic external irradiation of unit strength at one of its boundary surfaces. The results of calculations for the hemispherical reflectivity and absorptivity of the slab for $\omega = 0.7$ are given in Table 2 for five different scattering laws. The absorbed portion for case A is 0.5815 as compared to 0.5925 for the isotropic case. On the other hand, the absorption for forward scattering is 0.6181 for case B, 0.6195 for case C and 0.6205 for case D. It appears that with $\omega = 0.7$ considered here, forward scattering increases absorption in the medium. The stronger the forward scattering, the greater the absorption in the medium.

Figures 6 and 7 show the effects of anisotropic scattering on the propagation of the melt front for $\omega$ of 0.7 and 0.9, respectively. With backward scattering, case A, melting occurs more slowly than the isotropic case. On the other hand, with forward scattering, cases B, C and D, melting occurs faster than the isotropic case. Furthermore, the more forward the scattering, the faster the melting. For example, in Figs 6 and 7, the melting occurs faster with case D than case C. This is compatible with the conclusion reached above for the case of purely radiative heat transfer; that is, the stronger the forward scattering the more the absorption of radiation by the medium.

Figures 8 and 9 show the effects of anisotropic scattering on the propagation of the solidification front for $\omega$ of 0.7 and 0.9, respectively. The same conclusions reached above for melting are also applicable for solidification. Again, the backward scattering retards the solidification while the forward scattering enhances it. The more forward the scattering, the faster the rate of solidification.

Figure 10 illustrates the effects of the single scattering albedo, $\omega$, on the rate of propagation of the melt front at fixed times. At time $\xi = 0.7$, the melt rate decreases continuously for both isotropic and the backward scattering, case A, with increasing albedo. The melt rate is slower than the isotropic case with backward scattering (case A), but faster than the isotropic case with forward scattering (case C). All three cases converge to that of pure absorption, for $\omega = 0.0$; and

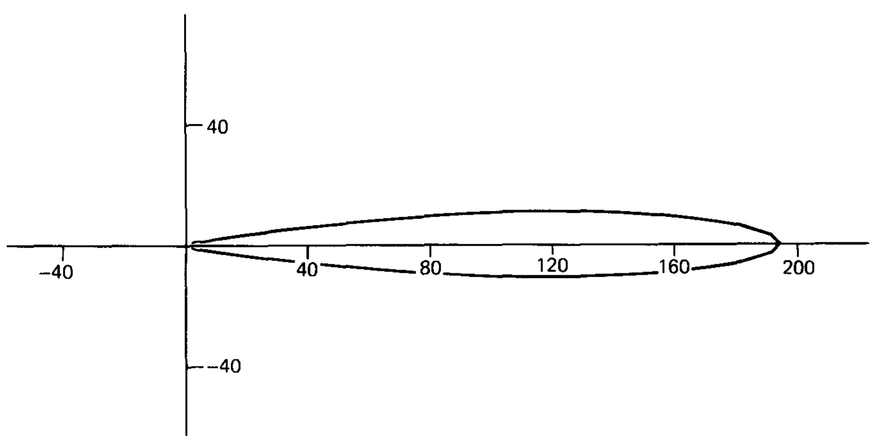


FIG. 4. The phase diagram for forward scattering with $n = 1.15$, $X_D = 15.0$ (Table 1, case C).

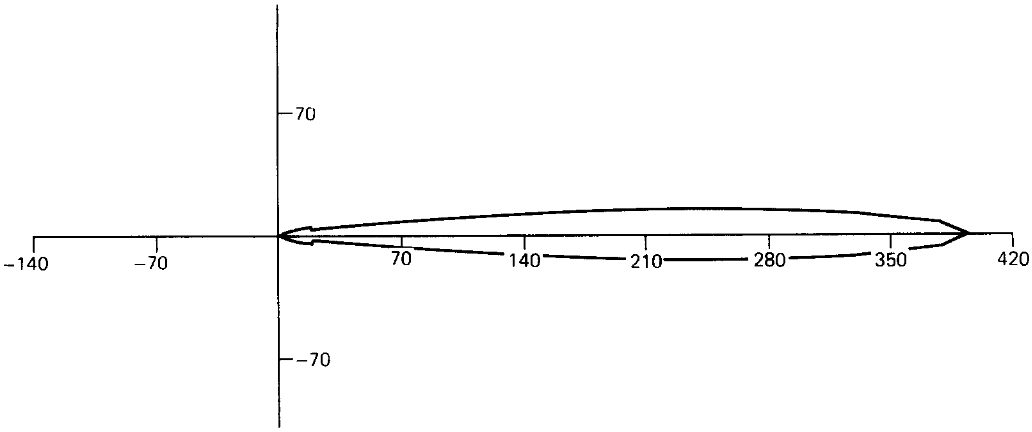


FIG. 5. The phase diagram for forward scattering with $n = 0.9$, $X_D = 25.0$ (Table 1, case D).

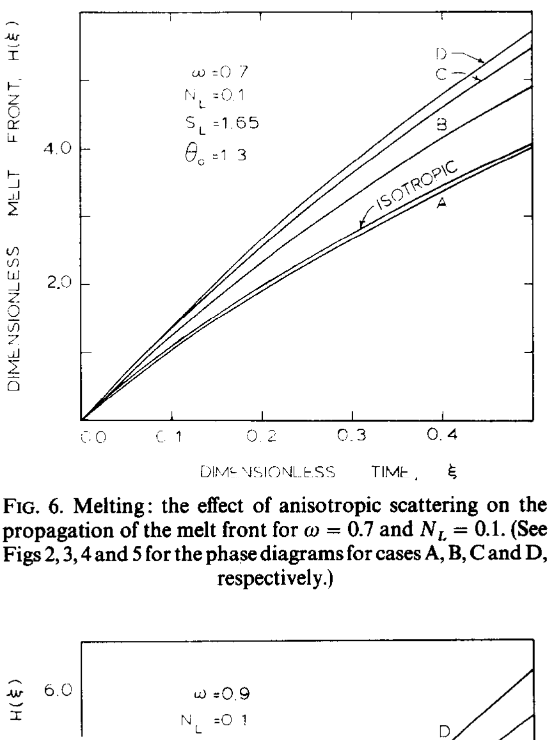


FIG. 6. Melting: the effect of anisotropic scattering on the propagation of the melt front for $\omega = 0.7$ and $N_L = 0.1$. (See Figs 2, 3, 4 and 5 for the phase diagrams for cases A, B, C and D, respectively.)

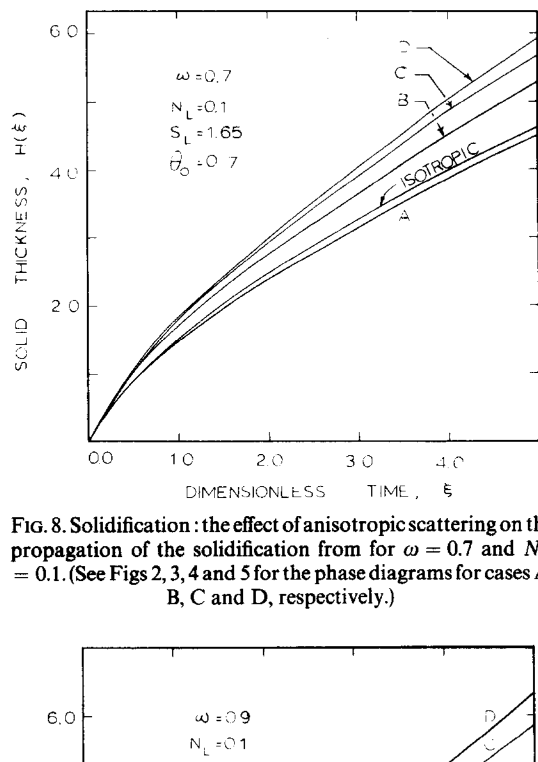


FIG. 8. Solidification: the effect of anisotropic scattering on the propagation of the solidification from for $\omega = 0.7$ and $N_L = 0.1$. (See Figs 2, 3, 4 and 5 for the phase diagrams for cases A, B, C and D, respectively.)

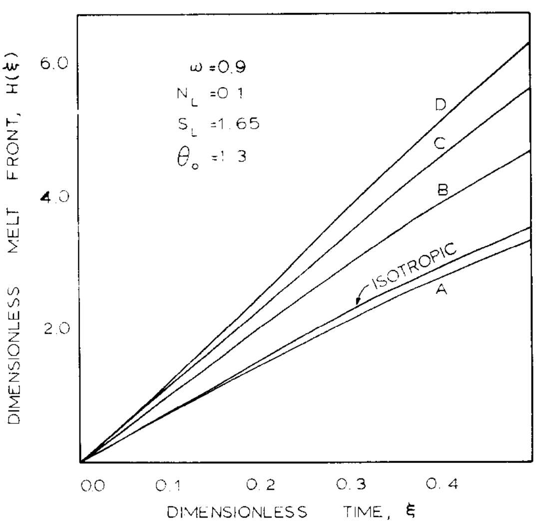


FIG. 7. Melting: the effect of anisotropic scattering on the propagation of the melt front for $\omega = 0.9$ and $N_L = 0.1$. (See Figs 2, 3, 4 and 5 for the phase diagrams for cases A, B, C and D, respectively.)

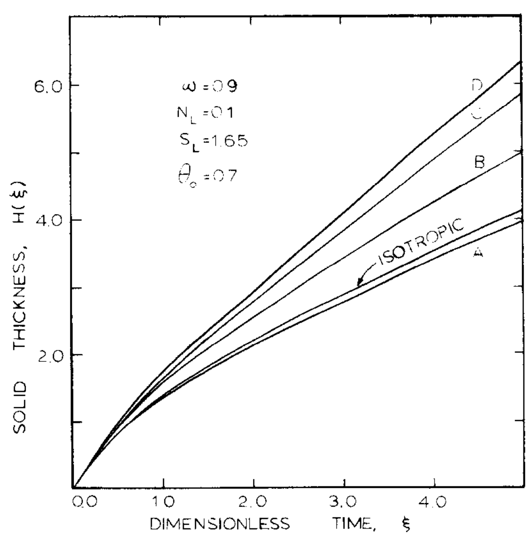


FIG. 9. Solidification: the effect of anisotropic scattering on the propagation of the solidification front for $\omega = 0.9$ and $N_L = 0.1$. (See Figs 2, 3, 4 and 5 for the phase diagrams for cases A, B, C and D, respectively.)

Table 2. Effect of anisotropic scattering on radiative transfer in a plane slab of optical thickness 2.0, with transparent boundaries, subjected to isotropic radiation at one of its boundary surfaces

| Albedo $\omega$ | Case | Hemispherical reflectivity | Hemispherical transmissivity | Absorptivity |
|---|---|---|---|---|
| | A (backward) | 0.2805 | 0.1380 | 0.5815 |
| | Isotropic | 0.2517 | 0.1558 | 0.5925 |
| 0.7 | B (forward) | 0.2622 | 0.1197 | 0.6181 |
| | C (forward) | 0.0447 | 0.3358 | 0.6195 |
| | D (forward) | 0.0097 | 0.3698 | 0.6205 |

approach to that of pure conduction (i.e. no radiation) as $\omega$ approaches unity.

The melting rate for the case C at different times are also shown on Fig. 10. At times $\xi = 0.1$ and 0.25, the thickness of the melt layer is small; thus, both the two-phase and solid regions are close to the heated wall and the effects of the forward scattering of the radiation are more pronounced. At larger times the thickness of the melt layer first increases with increasing $\omega$ because of the deeper penetration of the radiation due to the highly forward scattering; then as $\omega$ approaches 1.0, the melt layer thickness decreases because radiation effects are weakened as a result of reduced absorption and eventually the melting approaches that of pure conduction. For example, at time $\xi = 0.7$, the melt thickness first decreases slightly with increasing albedo and then starts increasing with increasing albedo. A peak is reached between $\omega = 0.81$ and $\omega = 0.94$, where the melt thickness is even slightly higher than that with pure absorption. As the albedo approaches 1.0, the melt rate decreases and approaches to that of pure conduction.

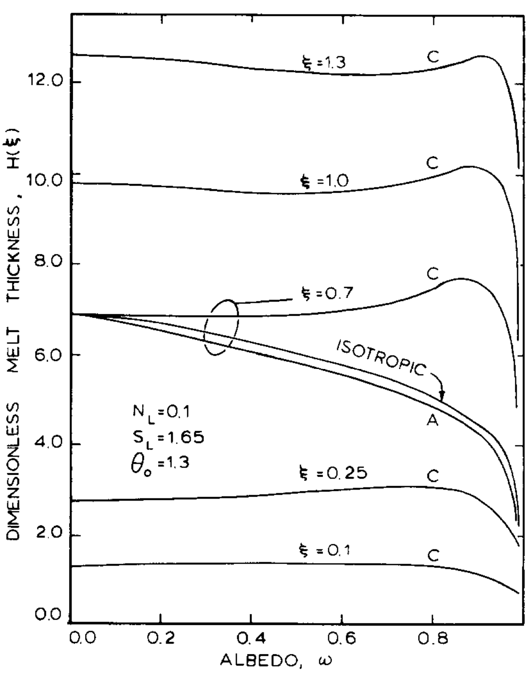


FIG. 10. Melting: the effect of albedo, $\omega$, on the melt layer thickness for fixed time $\xi$. (See Figs 2 and 4 for the phase diagrams for cases A and C, respectively.)

*Acknowledgement*—One of the authors (MNO) gratefully acknowledges the hospitality of ETH-Zürich during his visit. This work was supported in part through the National Science Foundation Grant No. MEA-81 10705.

## REFERENCES


1. R. N. Smith, T. E. Ebersole and E. P. Griffith, Heat exchanger performances in latent heat thermal energy storage, *ASME J. Solar Energy Engng* **102**, 112–118 (1980).
2. R. R. Gilpin, R. B. Robertson and B. Singh, Radiative heating in ice, *ASME J. Heat Transfer* **99**, 227–232 (1977).
3. G. E. Giles, J. R. Kirkpatrick and R. F. Wood, Laser annealing of solar cell wafers, *ASME Paper No. 80-HT-13* (1980).
4. H. S. Carslaw and J. C. Jaeger, *Conduction of Heat in Solids*. Oxford University Press, London (1959).
5. M. N. Özişik, *Heat Conduction*. Wiley-Interscience, New York (1980).
6. I. S. Habib, Solidification of a semi-transparent cylindrical medium by conduction and radiation, *J. Heat Transfer* **95**, 37–41 (1973).
7. I. S. Habib, Solidification of semi-transparent materials by conduction and radiation, *Int. J. Heat Mass Transfer* **14**, 2161–2164 (1974).
8. S. H. Chan, D. H. Cho and G. Kocamustafaogullari, Melting and solidification with internal radiative transfer—a generalized phase change model, *Int. J. Heat Mass Transfer* **26**, 621–633 (1983).
9. M. Abrams and R. Viskanta, The effects of radiative heat transfer upon the melting and solidification of semi-transparent crystals, *J. Heat Transfer* **96**, 184–190 (1974).
10. C. Cho and M. N. Özişik, Effects of radiation on the melting of a semi-transparent, semi-infinite medium, *Proc. 6th Heat Transfer Conf.* **3**, 373–378 (1978).
11. L. A. Diaz and R. Viskanta, Radiation induced melting of a semitransparent phase change material, Paper 82-0848, *AIAA/ASME 3rd Joint Thermophysics, Fluids, Plasma and Heat Transfer Conference*, St. Louis, Missouri, 7–11 June (1982).
12. L. A. Diaz and R. Viskanta, Melting of a slab of semitransparent material by irradiation from an external radiation source, Paper 81-1047, *AIAA 16th Thermophysics Conference*, Palo Alto, California, U.S.A. 23–25 June (1981).

13. C. M. Chu, G. C. Clark and S. W. Churchill, *Tables of Angular Distribution Coefficients for Light Scattering by Spheres*, University of Michigan Press, Ann Arbor, Michigan (1957).
14. M. N. Özişik, *Radiative Transfer*. John Wiley, New York (1973).
15. J. R. Mika, Neutron transport with anisotropic scattering, *Nucl. Sci. Eng.* **11**, 415–427 (1961).
16. C. E. Siewert and P. Benoist, The $F_N$ method in neutron transport theory, *Nucl. Sci. Eng.* **69**, 156–160 (1979).
17. C. E. Siewert, The $F_N$ method for solving radiative transfer problems in plane geometry, *Astrophy. Space Sci.* **58**, 131–137 (1978).
18. C. E. Siewert and F. O. Oruma, Particular solutions of the equation of transfer, *JQSRT* **22**, 223–227 (1981).

## APPENDIX

*Determination of radiation flux*

Assuming that the source the term $\theta^4(\tau, \xi)$ is available, the general solution of equations (6) and (7) can be written in the form [15]

$$\psi_L(\tau,\mu) = \sum_{j=0}^{M-1} [A(v_j)\phi_L(v_j,\mu)\,e^{-\tau/v_j} + A(-v_j)\phi_L(-v_j,\mu)\,e^{\tau/v_j}] + \int_{-1}^{1} A(v)\phi_L(v,\mu) \times e^{-\tau/v}\,dv + \psi_{LP}(\tau,\mu) \quad \text{(A1)}$$

$$\psi_S(\tau,\mu) = \sum_{j=0}^{M-1} [B(v'_j)\phi_S(v'_j,\mu)\,e^{-\tau/v'_j} + B(-v'_j)\phi_S(-v'_j,\mu)\,e^{\tau/v'_j}] + \int_{-1}^{1} B(v')\phi_S(v',\mu) \times e^{-\tau/v'}\,dv' + \psi_{SP}(\tau,\mu) \quad \text{(A2)}$$

where $A(\pm v)$ and $B(\pm v')$ are the expansion coefficients, $\psi_{iP}(\tau,\mu)$ with $i = L$ or $S$ is the particular solution of the equation of transfer, $\phi_S(\pm v'_j,\mu)$ and $\phi_L(\pm v_j,\mu)$ are the discrete eigenfunctions, $\phi_S(\pm v',\mu)$ and $\phi_L(\pm v,\mu)$ are the continuum eigenfunctions defined in the reference [15].

By using the full range orthogonality property of the eigenfunctions $\phi_i(v,\mu)$ equations (A1) and (A2) are transformed into the following system of singular integral equations:

$$\int_0^1 \mu\phi_L(-v,\mu)\psi_L(0,\mu)\,d\mu - \int_0^1 \mu\phi_L(v,\mu) \times \psi_L(0,-\mu)\,d\mu - e^{-H/v}\left[\int_0^1 \mu\phi_L(-v,\mu) \times \psi_L(H,\mu)\,d\mu - \int_0^1 \mu\phi_L(v,\mu)\psi_L(H,-\mu)\,d\mu\right] = \int_{-1}^{1} \mu\phi_L(-v,\mu)\psi_{LP}(0,\mu)\,d\mu - e^{-H/v} \times \int_{-1}^{1} \mu\phi_L(-v,\mu)\psi_{LP}(H,\mu)\,d\mu \quad \text{(A3)}$$

$$\int_0^1 \mu\phi_L(v,\mu)\psi_L(0,\mu)\,d\mu - \int_0^1 \mu\phi_L(-v,\mu) \times \psi_L(0,-\mu)\,d\mu - e^{H/v}\left[\int_0^1 \mu\phi_L(v,\mu)\psi_L(H,\mu)\,d\mu - \int_0^1 \mu\phi_L(-v,\mu)\psi_L(H,-\mu)\,d\mu\right] = \int_{-1}^{1} \mu\phi_L(v,\mu) \times \psi_{LP}(0,\mu)\,d\mu - e^{H/v}\int_{-1}^{1} \mu\phi_L(v,\mu)\psi_{LP}(H,\mu)\,d\mu \quad \text{(A4)}$$

$$\int_0^1 \mu\phi_S(-v',\mu)\psi_S(H,\mu)\,d\mu - \int_0^1 \mu\phi_S(v',\mu) \times \psi_S(H,-\mu)\,d\mu = \int_{-1}^{1} \mu\phi_S(-v',\mu)\psi_{SP}(H,\mu)\,d\mu. \quad \text{(A5)}$$

Instead of solving this system of equations directly, the basic concepts of the $F_N$ method [16, 17] is applied. Namely the exit distributions are represented by polynomials in the form

$$\psi_L(0,-\mu) = \sum_{j=0}^{M'} a_j\mu^j \quad \text{(A6)}$$

$$\psi_L(H,\mu) = \sum_{j=0}^{M'} y_j\mu^j \quad \text{(A7)}$$

$$\psi_S(H,-\mu) = \sum_{j=0}^{M'} b_j\mu^j \quad \text{(A8)}$$

where $a_j$, $y_j$, and $b_j$ are the expansion coefficients which are to be determined.

When the above polynomial representations equations are introduced into the integral equations (A3) to (A5) and the boundary conditions equation (8) are applied, we obtain a set of algebraic equations for the determination of the coefficients $a_j$'s, $y_j$'s and $b_j$'s. Here the particular solutions $\psi_{LP}(\tau,\mu)$ and $\psi_{SP}(\tau,\mu)$ depend on the functional form of the source term $\theta^4(\tau,\xi)$. A polynomial representation in the optical variable is assumed for the source term and the corresponding particular solutions are obtained from reference [18]. Once the resulting system of algebraic equations are solved and the coefficients $a_j$, $y_j$ and $b_j$, are determined, the net radiative heat flux $Q^r(\eta,\xi)$ and its derivative $\partial Q^r/\partial\eta$ are readily computed from their definitions.

$$Q^r|_H = \frac{1}{2}\int_{-1}^{1} \mu\psi(H,\mu)\,d\mu = \frac{1}{2}\sum_{j=0}^{M'} \frac{1}{j+2}(y_j - b_j) \quad \text{(A9a)}$$

$$\left.\frac{\partial Q^r}{\partial\eta}\right|_H = (1-\omega)\left[\psi_b(\theta) + \frac{1}{2}\int_{-1}^{1}\psi(H,\mu)\,d\mu\right] = (1-\omega)\left[1 - \frac{1}{2}\sum_{j=0}^{M'}\frac{1}{j+1}(y_j + b_j)\right] \quad \text{(A9b)}$$

$$Q^r|_{\eta=0} = \frac{1}{2}\int_{-1}^{1}\mu\psi_L(0,\mu)\,d\mu = \frac{1}{2}\left[\frac{\varepsilon_0\theta_0^4}{2} + (\rho_0 - 1)\sum_{j=0}^{M'}\frac{b_j}{j+2}\right] \quad \text{(A9c)}$$

## EFFETS DE LA DIFFUSION ANISOTROPE SUR LA FUSION ET LA SOLIDIFICATION D'UN MILIEU SEMI-INFINI ET SEMI-TRANSPARENT

**Résumé**—On étudie les effets de la diffusion anisotrope de rayonnement sur la fusion (solidification) d'un milieu semi-transparent et semi-infini à la température de fusion. Le modèle tient compte de la profondeur de pénétration du rayonnement dans la région isotherme et par suite d'une région biphasique entre les régions de liquide seul et de solide seul. Les résultats montrent que la diffusion anisotrope a un effet sensible sur la vitesse de propagation du front de fusion (solidification). La diffusion en retour retarde la fusion, tandis que la diffusion en avant l'accélère. Plus forte est la diffusion en avant, plus rapide est la fusion (solidification) du milieu.

## EINFLUSS DER ANISOTROPEN STREUUNG AUF DAS SCHMELZEN UND VERFESTIGEN EINES HALBUNENDLICHEN, HALBTRANSPARENTEN STOFFES

**Zusammenfassung**—Der Einfluß von anisotroper Streuung und Strahlung auf das Schmelzen (Verfestigen) eines halbunendlichen, halbtransparenten Stoffes, der sich auf Schmelztemperatur befindet, wird untersucht. Das Modell läßt zu, daß die Strahlung tief in das isotherme Gebiet eindringt und örtliches Schmelzen verursacht. Dadurch entsteht ein Zweiphasengebiet zwischen der reinen Flüssigkeit und dem reinen Feststoff. Die Ergebnisse zeigen, daß die anisotrope Streuung einen wesentlichen Einfluß auf die Ausbreitungsgeschwindigkeit der Schmelz-(Verfestigungs-) Front hat. Rückwärts-Streuung verzögert, Vorwärts-Streuung beschleunigt das Schmelzen. Je stärker die Vorwärts-Streuung ist, um so schneller geht der Schmelz-(Verfestigungs-) Vorgang vonstatten.

## ВЛИЯНИЕ АНИЗОТРОПНОГО РАССЕЯНИЯ НА ПЛАВЛЕНИЕ И ЗАТВЕРДЕВАНИЕ ПОЛУБЕСКОНЕЧНОЙ ПОЛУПРОЗРАЧНОЙ СРЕДЫ

**Аннотация**—Исследуется влияние анизотропного рассеяния излучения на плавление (затвердевание) полубесконечной полупрозрачной среды, находящейся при температуре плавления. Модель учитывает проникновение излучения вглубь изотермической области, где оно вызывает локальное плавление с образованием двухфазной зоны между чисто жидкой и чисто твердой областями. Результаты показывают, что анизотропное рассеяние оказывает существенное влияние на скорость распространения фронта плавления (затвердевания). Рассеяние назад замедляет плавление, а рассеяние вперед ускоряет его. Чем больше расстояние, на которое продвигается вперед рассеяние, тем быстрее происходит плавление (затвердевание) среды.